Surface & Coatings Technology 298 (2016) 1–6

Contents lists available at ScienceDirect

Surface & Coatings Technology

journal homepage: www.elsevier.com/locate/surfcoat

Nano-galvanic coupling for enhanced Ag^+ release in ZrCN-Ag films: Antibacterial application

S. Calderon V [a,d,*], I. Ferreri [a,b], M. Henriques [b], J.T.M. De Hosson [c], A. Cavaleiro [d], S. Carvalho [a,d]

[a] GRF-CFUM, Physics Department, University of Minho, 4800-058 Guimarães, Portugal
[b] CEB, Center of Biological Engineering, LIBRO – Laboratório de Investigação em Biofilmes Rosário Oliveira, University of Minho, Campus of Gualtar, 4700-057, Portugal
[c] Department of Applied Physics, University of Groningen, Zernike Institute for Advanced Materials, Nijenborgh 4, 9474 AG Groningen, The Netherlands
[d] SEG-CEMUC Mechanical Engineering Department, University of Coimbra, 3030-788 Coimbra, Portugal

ARTICLE INFO

Article history:
Received 1 February 2016
Revised 6 April 2016
Accepted in revised form 7 April 2016
Available online 10 April 2016

Keywords:
Silver ionization
Antibacterial
Nanoparticles
Galvanic couples
Sputtering
ZrCN

ABSTRACT

The antibacterial properties of materials developed for medical devices with embedded silver nanoparticles are enhanced by controlling the release of silver ions. In this study, a simple experimental procedure for the augmentation of the silver ion release from ZrCN-Ag coatings is described. The silver nanoparticles are embedded in an amorphous carbon matrix within the ZrCN coatings, to create nano-galvanic couples between the silver and the carbon phases. The galvanic couple promotes the oxidation of silver, and consequently, increases the silver release. It is demonstrated that coatings with a lower silver content, but integrating amorphous carbon phases, can release similar or even a larger amount of Ag^+ ions than those with higher Ag content having just ZrCN and Ag phases. The antibacterial tests demonstrate that coatings with silver nanoparticles encapsulated into amorphous phase reveal a larger bacterial zone of inhibition compared to samples with similar or lower silver content. However, it is shown that the antibacterial effect of the coatings not only depends on the ability for silver ion release, but also on the availability of silver nanoparticles on the surface.

1. Introduction

Silver nanoparticles (NPs) have been extensively used to provide antibacterial properties to several commercial products such as sportswear, toys and baby commodities [1]. A large number of papers were published during the last few years regarding silver NPs for attaining antimicrobial properties in various materials and for a considerably number of microorganisms, as e.g. [2–11]. Hsieh et al. [8], for instance, have shown an antibacterial effect against *Escherichia coli* (*E. coli*) on TaN samples with 1.6 to 10 at.% of silver in tests carried out for 24 h; they concluded that the dissolution of the silver prompts the antibacterial effect, with 80% of antibacterial efficiency for a sample with 10 at.% of silver. However, the amount of silver dissolved in the medium was not reported. Akhavan et al. [9] evaluated the influence of the shape of silver particles embedded in TiO_2 on the antibacterial effect against *E. coli* and the release of silver ions to the medium. It was found that the latter can be increased or reduced depending on the silver geometry, such as thin films, nanorods or nanoparticles. However, the amount of silver released and the antibacterial results cannot be directly correlated, since an acid solution was used for detecting the Ag^+, accelerating the silver ionization. Jamuna et al. [10] have demonstrated that very low concentrations of silver ions can show antibacterial behavior in Ag-TiO_2 coatings, against *Staphylococcus aureus* (*S. aureus*). In their study, the Ag^+ released is largely reduced after 4 days of immersion, reaching values not higher than ~28 ppb cm^{-2} of Ag^+ after 1 day of immersion in phosphate buffered saline solution.

On the other hand, Sant et al. [11] reported silver films prepared by magnetron sputtering in which the Ag^+ release depends on the morphology of the films. They also showed that the nanocrystalline silver films are more effective as antibacterial material against *S. aureus* due to an enhanced solute-defect coupling at specific grain boundaries that assist the metal ion release from the surface. The films released >1 ppm of silver ions after 1000 min of immersion. Indeed, for long term applications this phenomenon could generate toxicity problems.

These studies suggest that more than one parameter should be taken into consideration when evaluating and controlling the silver ion release. Particularly for ZrCN-Ag system, we have found in our previous work [12] a very low silver ion release, with a consequent lack of antibacterial activity against *Staphylococcus epidermidis*. This bacteria possess the ability to adhere to biodevices, being associated to prosthetic device-related infections [13], highlighting the importance of developing biomaterials with antibacterial capabilities against this *Staphylococcus*.

In this paper, we aim at presenting a methodology developed to increase the silver ion release for ZrCN-Ag films, which makes them potentially useful for surface modification of medical devices. This methodology can be adapted for other transition metal carbonitride

* Corresponding author at: Universidade do Minho, Dept. Física, Campus de Azurém, 4800-058 Guimarães, Portugal.
E-mail address: secave44@gmail.com (S. Calderon V).

http://dx.doi.org/10.1016/j.surfcoat.2016.04.019
0257-8972/

Table 1
Deposition parameters and compositional analysis of Zr-*C*-*N*-Ag coatings.

Sample	Ag current density [mA cm^{-2}]	C_2H_2 [sccm]	N_2 [sccm]	Thickness [μm]	Zr [%]	N [%]	C [%]	Ag [%]	O [%]	$\frac{C+N}{Zr}$
Ag6	0.25	1.2	3	1.8	46	24	18	6	6	0.9
Ag7	0.25	1.2	9	1.1	32	39	18	7	4	1.8
Ag9	0.5	2.4	3	1.6	35	18	29	9	9	1.4
Ag13	0.5	2.4	9	1.5	21	30	27	13	9	2.8
Ag20	0.75	1.2	3	2.0	38	20	16	20	6	1.0

systems containing silver. Specifically, we will present results on the influence of the matrix composition and the structural properties of ZrCN-Ag coatings on the release of silver ions.

2. Material and methods

2.1. Material production

The films were deposited by dual reactive magnetron sputtering onto 316L stainless steel (SS316L) substrates, using 60 sccm of Ar flux as inert gas, while the reactive gases (C_2H_2 and N_2) were varied to alter the amount of amorphous carbon in the coatings, as shown in Table 1. The Zr target current density was kept constant for all depositions at 10 mA cm^{-2}, while the Ag target current density was varied between 0.25 and 0.75 mA cm^{-2}. The distance between the substrates and the target (70 mm), as well as the temperature (373 K) and the substrate bias voltage (−50 V) remained constant during the depositions. For a more detailed description of the deposition process reference is made to our previous publication [12].

The substrates were cleaned in ultrasonic baths successively in distilled water, ethanol and acetone, for 10 min in each fluid, and etched with argon ions before deposition.

2.2. Glow discharge optical emission spectroscopy (GD-OES)

The profile of the in-depth silver distribution was evaluated, before and after immersing the samples in 0.9% NaCl during 240 h, using a glow discharge optical emission spectrometer (GD-OES - Jobin Yvon RF GD Profiler) equipped with a 4 mm diameter anode and operating at a discharge pressure of 650 Pa and a radio frequency power of 40 W. The emission lines detected were oxygen (130 nm), nitrogen (149 nm), carbon (156 nm), silver (328 nm), nickel (341 nm), chromium (425), zirconium (339 nm) and iron (271 nm). The calibration of light elements such as N was carried out as explained in [14]. The calibrations of oxygen and carbon were carried out with standards materials.

2.3. Transmission electron microscopy (TEM) and high resolution TEM (HR-TEM)

High-resolution (HR-TEM) images of the samples in cross-section were acquired in a JEM 2010F transmission electron microscope, operating at 200 kV, equipped with an EDS system. The high-resolution images were recorded around Scherzer defocus, i.e. −64 nm. Fast Fourier transformation (FFT) was carried out using a digital micrograph software package (Gatan, USA) to obtain the digital diffraction pattern in high resolution TEM images. The samples were prepared in cross-section following the methodology described elsewhere [15].

2.4. Scanning electron microscopy (SEM)

SEM images were obtained using a high resolution NanoSEM - FEI Nova 200 equipped with a field emission gun (FEG). The microscope was operated in high vacuum mode at an acceleration voltage of 10 kV with a working distance of around 5 mm. The micrographs were obtained with a backscattered electron detector.

2.5. Inductively coupled plasma optical emission spectroscopy (ICP-OES)

For detecting the release of silver ions, 4 cm^2 samples were immersed into a 50 ml vessel, containing 30 ml of 0.9% NaCl at room temperature. Thereafter, 1.5 ml of the solution was taken out at different times and reserved for inductively coupled plasma optical emission spectrometry (ICP-OES) analysis. Tests were carried out in an ICP-OES spectrometer PERKIN ELMER OPTIMA 8000, within a period of 30 days. In order to avoid silver precipitation, the solutions were maintained in the dark until ICP evaluation. Two calibration curves were prepared using a silver standard solution for ICP (silver, plasma standard solution, spec pure, Ag 1000 μg ml^{-1}). The first calibration curve was prepared in HNO_3 acid, because this is the matrix in which the silver is stabilized, the second calibration curve was prepared in NaCl 0.9% in order to mimic the experimental conditions used for the samples. Both calibration curves showed indistinguishable results. The presence

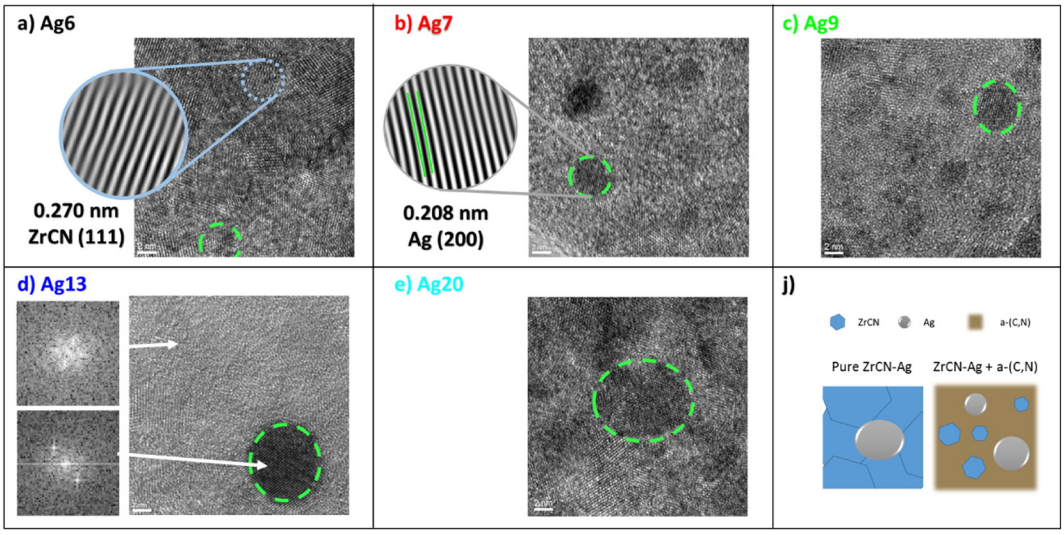

Fig. 1. High resolution transmission electron microscopy images of the Zr-*C*-*N*-Ag coatings. The dashed lines identify a silver nanoparticle in the Zr-C-N matrix a) Ag6, b) Ag7, c) Ag9, d) Ag13, e) Ag20 and f) scheme of the phase distribution. FFT and inverse FFT were used to identify the phases, exemplified in a), b) and d). (For interpretation of the references to color in this figure, the reader is referred to the web version of this article.)

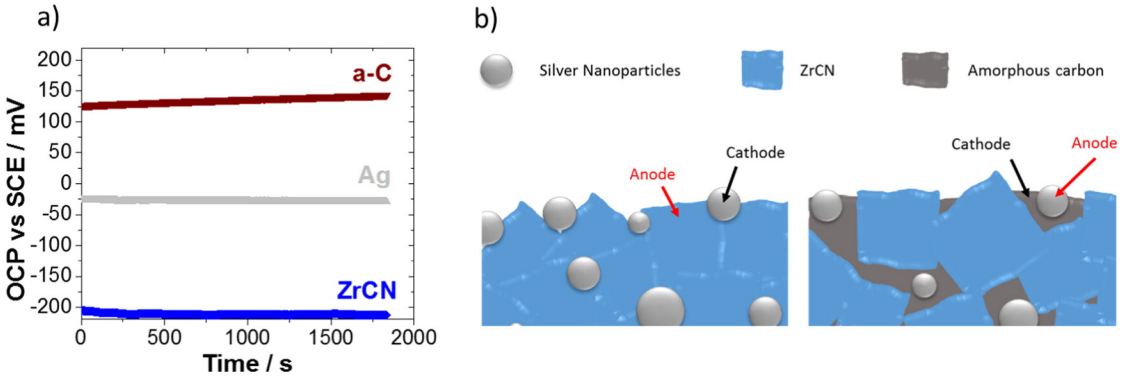

Fig. 2. a) Open circuit potential of pure Ag, ZrCN and a-C films immersed in 0.9% NaCl and b) scheme of phase distribution and determination of anode and cathode in the electrochemical reaction triggered in NaCl 0.9% for different phases.

of Zr ions was also evaluated in the solution after immersion, and both calibration curves were also prepared; however, no presence of Zr was detected in the solution after 336 h of immersion.

2.6. Antibacterial test

The antibacterial properties of the coating were assessed by means of the zone of inhibition (ZOI) test [7]. A single colony of *S. epidermidis* (IE186 strain, a clinical isolate belonging to the CEB Biofilm Group collection) was inoculated in 20 ml of Tryptic Soy Broth (TSB, Merck) for 18 h at 37 °C, and 120 rpm. The inoculum bacteria concentration was adjusted to a concentration of 1×10^7 colony forming units (CFU) ml^{-1} by correcting the optical density (OD) to 1.0 at 640 nm. The cellular suspension was added to cooled (50 °C) TSB agar (Merck) (TSA) (1:14 ml) and placed into sterile plastic Petri dishes. After medium solidification, samples of ~1 cm^2 (previously sterilized in UV light for 30 min) were placed on the agar plates and cultured for 24 h, at 37 °C. After the incubation period, images of the Petri dishes were acquire by an Image Lab™ software and the ZOI was measured using ImageJ software.

3. Results and discussion

The materials reported were characterized and the results can be found in previous publications [12,15]. In short, the results demonstrate that the coatings are composed of a mixture of phases of ZrC_xN_{1-x} crystalline phase (ZrCN), metallic silver nanoparticles, as well as an amorphous carbon phase (a-(C,N)), in agreement with the ratio of (C + N)/Zr atomic percentages, reported in Table 1. The excess of carbon into the films (a-(C,N) phases) is attained throughout a hybrid process of magnetron sputtering and plasma enhanced chemical vapor deposition processes, in which the quantity of reactive acetylene exceeds the amount able to react with the Zr atoms to form ZrCN. The remaining gas reacts with the surface, forming carbon phases. The process depends not only on the amount of C_2H_2 introduced into the chamber, but also on the N_2 and Zr available to react and form ZrCN.

The silver content varied from 6 to 20 at.% and is accompanied by the variation of the carbon and nitrogen in the coatings, as summarized in Table 1. The silver content will be used as the sample notation throughout the document.

The C + N/Zr ratio shown in Table 1 is lower than 1 for samples Ag6 and Ag20 and only ZrCN and Ag phases should exist, whereas the coexistence of ZrCN, amorphous carbon phase and silver is expected for samples Ag7, Ag9 and Ag13, reaching the conditions for the nano-galvanic coupling. Nonetheless, in order to corroborate the silver encapsulation into these ceramic phases and their distribution, HR-TEM images were acquired in all the coatings.

Fig. 1 shows characteristic HR-TEM images of the films. The phases were identified by calculating the FFT and IFFT of the images in specific regions and compared with the interplanar distance of the phases (ZrCN and Ag FCC crystalline structures), as exemplified in Fig. 1a, b and d. The areas highlighted in green dashed lines correspond to silver nanoparticles. For samples Ag6 and Ag20 (Fig. 1a and e), silver nanoparticles are surrounded by a well-organized crystalline phase, which corresponds to ZrCN. On the other hand, samples Ag7, Ag9 and Ag13 (Fig. 1b–d) show the existence of amorphous carbon phases encapsulating the

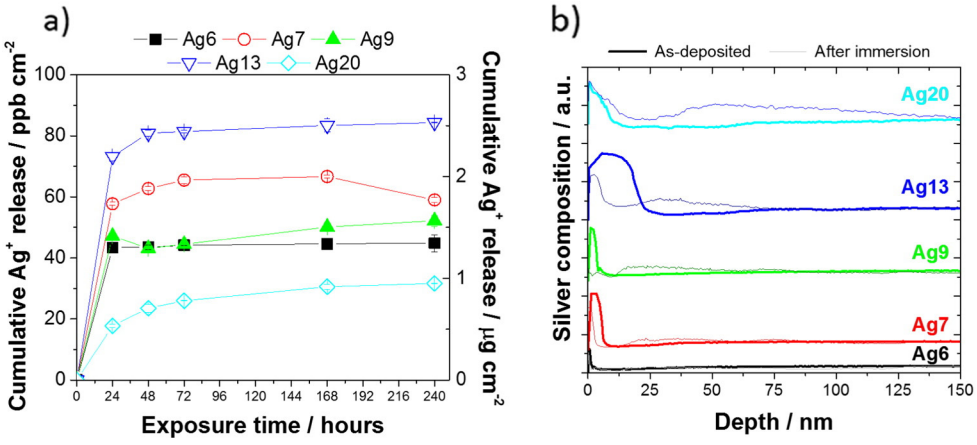

Fig. 3. a) Silver ion release of the samples as a function of immersion time in NaCl 0.9% and b) Ag GD-OES depth profile near surface (<150 nm) for the coatings before and after immersion in NaCl 0.9%.

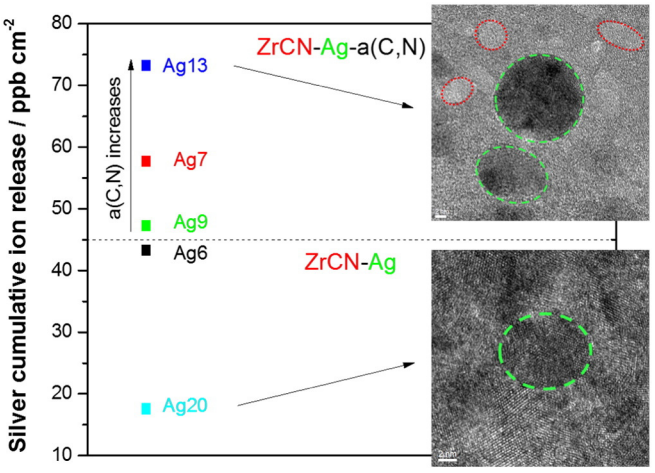

Fig. 4. Comparison between the silver ion release after 24 h obtained by ICP and the phase distribution images by HR-TEM.

silver nanoparticles, as schematized in Fig. 1j. This encapsulation is expected to offer electrical contact between the silver nanoparticles and the conductive ceramic phases (ZrCN and a-(C,N)), which activate different electrochemical reactions when immersed in an electrolyte, promoting the phases oxidation or reduction, depending on their reduction potentials.

The open circuit potential (OCP) of each phase was measured, in the same NaCl 0.9%, for pure silver, pure amorphous carbon and pure ZrCN films; the average values after one hour of immersion were −0.02 V, +0.142 V and −0.21 V, respectively (cf. Fig. 2a). These potentials confirm that silver can act as the cathode (higher OCP), when connected to pure ZrCN. This is the case of the microstructures of samples Ag6 and Ag20. However, if silver is surrounded by an amorphous carbon phase, as for Ag7, Ag9 and Ag13 samples, silver behaves as the anode of the reaction (lower OCP), promoting a higher silver ion release. Therefore, silver is the anode or the cathode in the electrochemical cell, when electrically in contact with the ceramic phases (a:C or ZrCN, respectively), as schematically shown in Fig. 2b.

In order to corroborate this behavior, *ICP-OES* measurements were carried out to determine the amount of silver released.

3.1. Silver ion release

Fig. 3a displays the cumulative silver ion release obtained by ICP-OES as a function of the immersion time of the samples in NaCl 0.9%. The results revealed a fast release in the first 48 h of immersion, reaching an almost constant ion concentration in the fluids. It indicates a very slow ion release from the samples after this period. This characteristic behavior was also found in TiO_2-Ag samples [9] and in Ag nanoparticles in natural water [16].

The amount of silver ion released to the electrolyte has demonstrated that leaching is not dependent on the amount of silver present in the coatings. Samples Ag6 and Ag20, for instance, possess the lowest cumulative silver release, while samples with excess of carbon (Ag7, Ag9 and Ag13) show higher release. Similar trends can be observed by GD-OES before and after immersion, as shown in Fig. 3b, confirming the ICP results. In addition, GD-OES results show an unexpected accumulation of silver on the surface for sample Ag20, and redistribution of silver from the interior to the films surface in all the samples.

The results confirm our hypothesis that the matrix surrounding the silver controls silver ion release. When amorphous carbon phases are present in the films, the silver nanoparticles tend to be encapsulated by these phases, while for pure ZrCN-Ag films, Ag nanoparticles are surrounded by the crystalline ZrCN, as shown in Fig. 4.

3.2. Bacterial zone of inhibition test

The ZOI test was used to evaluate the antimicrobial ability of the films, against *S. epidermidis* (Fig. 5) and its correlation with the silver ion release in the coatings. It must be emphasized that although silver ionization in NaCl may differ from the Ag^+ released in the bacteria agar [12], the trends are expected to be similar in each electrolyte.

Fig. 5a displays the samples after the bacteria incubation period (24 h). Around the edges of the samples, a small clearer area (Fig. 5c) can be observed, which corresponds to the zone where bacterial growth does not occur. A pure ZrCN sample has been used as a control in order to observe the absence of the ZOI (labeled 0 at.%). For this sample, a very intense bright line (Fig. 5d) is observed near the edge, corresponding to the growth of bacteria accumulated in its lateral side. Similarly, sample 6 at.% did not show a visible ZOI and no ZOI can be quantified. Samples Ag7, Ag9, Ag 13 and Ag20 showed a

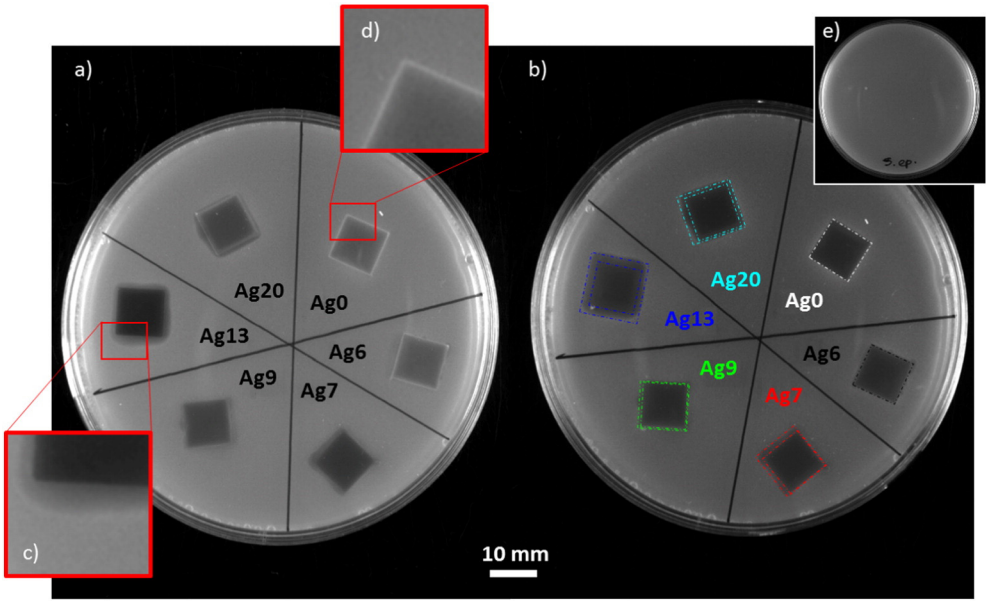

Fig. 5. Zone of inhibition assays for Zr-*C*-*N*-Ag coatings a) raw image after 24 h of the test, b) highlighting the ZOI area. The inset c) shows an example of the ZOI in sample Ag13, inset d) the lack of ZOI in Ag0 and inset e) a growth control Petri dish for the *S. epidermidis*.

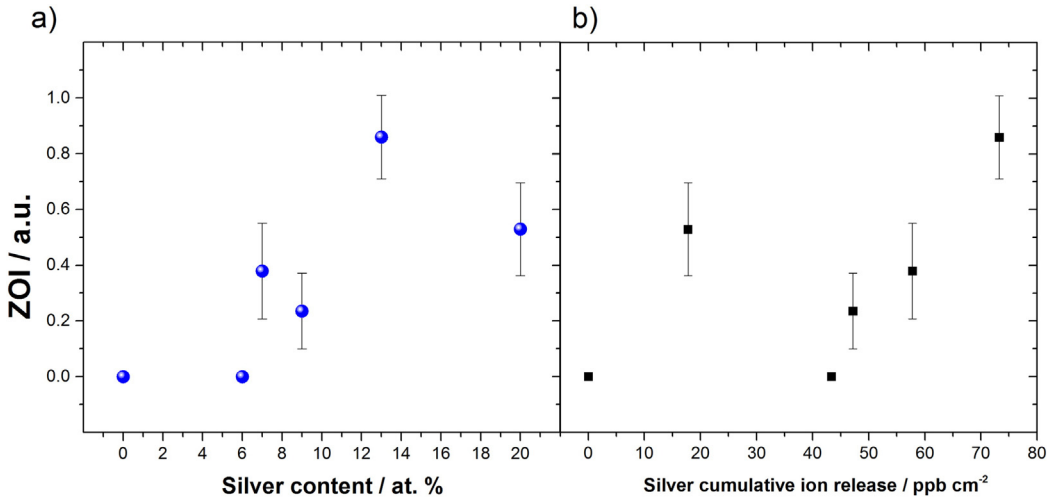

Fig. 6. Normalized zone of inhibition area for Zr-*C*-*N*-Ag coatings as a function of a) silver content and b) silver ion release.

more defined inhibition zones, which are quantified using a normalized area of inhibition, Eq. (1).

$$\text{Normalized ZOI} = \frac{\text{Area}_{ZOI} - \text{Area}_{Sample}}{\text{Area}_{Sample}} \quad (1)$$

where the Area_{ZOI} and Area_{sample} correspond to the external and internal rectangles drawn in Fig. 5b, respectively, for each sample.

The result of the normalized ZOI is shown in Fig. 6 as a function of the silver content in films and the silver ion release. Fig. 6a reveals that the size of the bacterial zone of inhibition is not evidently related to the silver content in the coatings, to some extent expected due to the lack of correlation between the silver content and the silver ion release, demonstrated in the previous section. On the other hand, although the silver ion release seems to be directly correlated with the ZOI area for most of the samples (right side of Fig. 6b), unexpectedly the sample with the lowest Ag^+ release (Ag20) exhibits a comparable ZOI to the intermediate silver ion release sample (Ag7).

Thus, in order to understand the reason for the sample Ag20 to exhibit a comparable ZOI against *S. epidermidis* in spite of its lower Ag^+ ion release, the surface before and after immersion was studied by scanning electron microscopy.

Fig. 7 shows the top-view images taken by SEM before and after sample immersion in the electrolyte. The micrographs were taken using a backscattering electron detector in order to achieve a better contrast of the surface composition. Before immersion, bright nanoparticles corresponding to silver (heavier element) are only clearly observed in sample Ag20. This behavior has been previously reported in others ceramic-Ag coatings [17], in which the silver segregates to the surface only for high silver content.

After immersion in NaCl 0.9% the segregation of silver is again more evident for Ag20, despite of the fact that very small nanoparticles are observed in samples Ag7 and Ag13.

The size distribution of the silver nanoparticles is shown in Fig. 8. The figure reveals an average size of the silver nanoparticles, which is more related to the phase composition than to the silver content in the films. In fact the nanoparticles size decreases with increasing

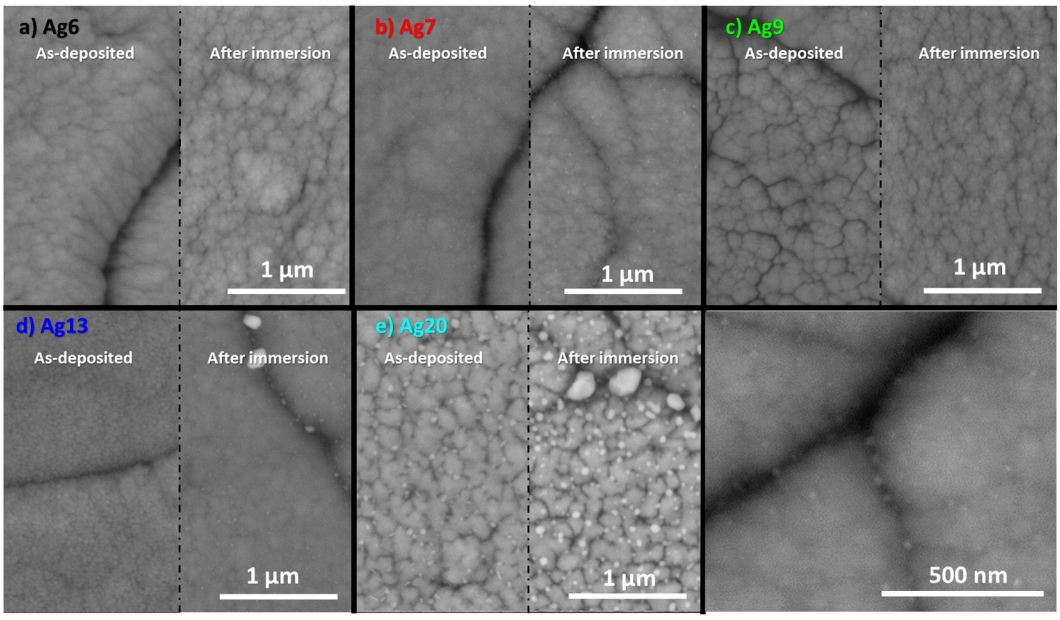

Fig. 7. Coatings surface SEM images in backscattering mode before and after immersion in NaCl 0.9% for different silver content a) 6 at.%, b) 7 at.%, c) 9 at.%, d) 13 at.% and e) 20 at.%. f) Amplification of Ag7 surface after immersion exemplify the Ag nanoparticles observed.

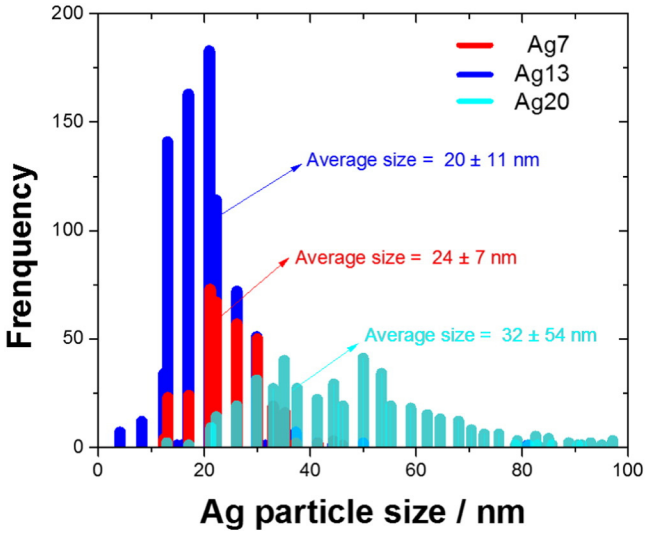

Fig. 8. Histograms for the size of silver nanoparticles formed after immersion in samples with 7 at.%, 13 at.% and 20 at.% of silver.

carbon phase content in the sequence Ag20-Ag7-Ag13 (Table 1). This is related to the fact that small size particles dissolve easier whereas, those with larger sizes exhibit Ostwald ripening. In fact, in samples with a lower amount of amorphous carbon phases, the silver is more likely to be in contact with the ZrCN phase, and therefore, acting as a cathode, reducing the silver ions and accelerating the growing process.

Taking into consideration both the silver ion release and the amount of silver nanoparticles on the surface of the samples, the antibacterial behavior of the coatings should be a compromise between different factors, as follows: i) the ability of the material to form silver particles on the surface, ii) the size of the silver particles and iii) the amount of silver ions released. In the first case, for example, sample Ag20 show the lowest silver ion release; however, it shows a ZOI area size located between those of Ag7 and Ag13. On the other hand, samples Ag6 and Ag9, with higher silver release, compared to Ag20 sample, exhibit lower or none ZOI. This behavior may be associated to the amount of silver present on the surface.

In the second and third scenarios, samples Ag7 and Ag13, with dissimilar silver segregation to the surface when compared to sample Ag20, show a comparable (Ag7) or larger (Ag13) ZOI area with respect to Ag20. Therefore, there is not an obvious correlation between the amounts of Ag segregated to the surface and the antibacterial effect, indicating that an additional factor should be taken into consideration. Lower size nanoparticles have been demonstrated to increase the antibacterial activity of the silver, due to either their ability to penetrate the bacteria wall [18] or the increase of the silver ion release [19], the latter being the preferred for interpreting the results achieved in this study. Additional studies should be performed with systems where the separation of those factors can be easily achieved.

Finally, the method used for the antibacterial evaluation should be also taken into account. In fact, it highly depends on the sample surface, which is placed directly in contact with the bacteria broth; this is different from the procedure where species need to be dissolved in the agar. Thus, the silver segregation may play an important role on the antibacterial activity of the coatings, since the silver segregation on the coatings surface will provide the system with enough antibacterial agent to act against the bacteria. In addition, this mechanism may be exploited as a self-controlling material to provide antimicrobial activity. This is due to the fact that despite of being an antibacterial surface, the silver ion release is kept below the toxicity levels. Therefore it may prevent the contamination of the environment in which the material is located.

4. Conclusions

ZrCN-Ag coatings with nano-galvanic couples formed between the silver nanoparticles and conductive ceramic matrix (ZrCN and amorphous carbon) were produced by magnetron sputtering. Nano-galvanic couples can enhance the silver ion release from the coatings, promoting a larger zone of bacteria inhibition against *S. epidermidis*. The results demonstrate that when silver is encapsulated by amorphous carbon phases, the silver ion release increased, compared to silver surrounded by pure ZrCN phases. These nano-galvanic couples enhance the antibacterial effect, indicating that it is possible to achieve similar or larger bacterial zone of inhibition with lower amount of antibacterial agent, by encapsulating the silver in amorphous carbon phases.

Acknowledgements

This research is partially sponsored by FEDER funds through the program COMPETE - Programa Operacional Factores de Competitividade and by Portuguese national funds through FCT-Fundação para a Ciência e a Tecnologia, under the projects ANTIMICROBCOAT - PTDC/CTM/102853/2008 and in the framework of the Strategic Projects PEST-C/FIS/UI607/2011", UID/EMS/00285/2013 and SFRH/BD/80947/2011.

References

[1] C. Marambio-Jones, E.V. Hoek, A review of the antibacterial effects of silver nanomaterials and potential implications for human health and the environment, J. Nanoparticle Res. 12 (2010) 1531–1551.
[2] A. Betts, D. Dowling, M. McConnell, C. Pope, The influence of platinum on the performance of silver-platinum anti-bacterial coatings, Mater. Des. 26 (2005) 217–222.
[3] A.M. El-Kady, A.F. Ali, R.A. Rizk, M.M. Ahmed, Synthesis, characterization and microbiological response of silver doped bioactive glass nanoparticles, Ceram. Int. 38 (2011) 177–188.
[4] C.N. Lok, C.M. Ho, R. Chen, Q.Y. He, W.Y. Yu, H. Sun, P.K.H. Tam, J.F. Chiu, C.M. Che, Silver nanoparticles: partial oxidation and antibacterial activities, J. Biol. Inorg. Chem. 12 (2007) 527–534.
[5] H. Cao, X. Liu, F. Meng, P.K. Chu, Biological actions of silver nanoparticles embedded in titanium controlled by micro-galvanic effects, Biomaterials 32 (2011) 693–705.
[6] D. Dowling, A. Betts, C. Pope, M. McConnell, R. Eloy, M. Arnaud, Anti-bacterial silver coatings exhibiting enhanced activity through the addition of platinum, Surf. Coat. Technol. 163 (2003) 637–640.
[7] P.J. Kelly, H. Li, P.S. Benson, K.A. Whitehead, J. Verran, R.D. Arnell, I. Iordanova, Comparison of the tribological and antimicrobial properties of CrN/Ag, ZrN/Ag, TiN/Ag, and TiN/Cu nanocomposite coatings, Surf. Coat. Technol. 205 (2010) 1606–1610.
[8] J. Hsieh, C. Tseng, Y. Chang, S. Chang, W. Wu, Antibacterial behavior of TaN–Ag nanocomposite thin films with and without annealing, Surf. Coat. Technol. 202 (2008) 5586–5589.
[9] O. Akhavan, E. Ghaderi, Capping antibacterial Ag nanorods aligned on Ti interlayer by mesoporous TiO2 layer, Surf. Coat. Technol. 203 (2009) 3123–3128.
[10] K. Jamuna-Thevi, S. Bakar, S. Ibrahim, N. Shahab, M. Toff, Quantification of silver ion release, in vitro cytotoxicity and antibacterial properties of nanostructured Ag doped TiO2 coatings on stainless steel deposited by RF magnetron sputtering, Vacuum 86 (2011) 235–241.
[11] S. Sant, K. Gill, R. Burrell, Nanostructure, dissolution and morphology characteristics of microcidal silver films deposited by magnetron sputtering, Acta Biomater. 3 (2007) 341–350.
[12] V. S. Calderon, I. Ferreri, R.E. Galindo, M. Henriques, A. Cavaleiro, S. Carvalho, Electrochemical vs antibacterial characterization of ZrCN-Ag coatings, Surf. Coat. Technol. 275 (2015) 357–362.
[13] I. Carvalho, M. Henriques, J.C. Oliveira, C.F.A. Alves, A.P. Piedade, S. Carvalho, Influence of surface features on the adhesion of *Staphylococcus epidermidis* to Ag–TiCN thin films, Sci. Technol. Adv. Mater. (2016).
[14] R. Escobar Galindo, N.K. Manninen, C. Palacio, S. Carvalho, Advanced surface characterization of silver nanocluster segregation in Ag–TiCN bioactive coatings by RBS, GDOES, and ARXPS, Anal. Bioanal. Chem. 405 (2013) 6259–6269.
[15] V. S. Calderon, A. Cavaleiro, S. Carvalho, Chemical and structural characterization of ZrCNAg coatings: XPS, XRD and Raman spectroscopy, Appl. Surf. Sci. 346 (2015) 240–247.
[16] J. Dobias, R. Bernier-Latmani, Silver release from silver nanoparticles in natural waters, Environ. Sci. Technol. 47 (2013) 4140–4146.
[17] P. Basnyat, B. Luster, Z. Kertzman, S. Stadler, P. Kohli, S. Aouadi, J. Xu, S.R. Mishra, O.L. Eryilmaz, A. Erdemir, Mechanical and tribological properties of CrAlN-Ag self-lubricating films, Surf. Coat. Technol. 202 (2007) 1011–1016.
[18] I. Sondi, B. Salopek-Sondi, Silver nanoparticles as antimicrobial agent: a case study on *E. coli* as a model for Gram-negative bacteria, J. Colloid Interface Sci. 275 (2004) 177–182.
[19] W.K. Jung, H.C. Koo, K.W. Kim, S. Shin, S.H. Kim, Y.H. Park, Antibacterial activity and mechanism of action of the silver ion in *Staphylococcus aureus* and *Escherichia coli*, Appl. Environ. Microbiol. 74 (2008) 2171–2178.